ISSN 1674-1056
http://cpb.iphy.ac.cn
http://iopscience.iop.org/cpb
中国物理 B
Chinese Physics
中国物理
Chinese Physics B

Physical manipulation of ultrathin-film optical interference for super absorption and two-dimensional heterojunction photoconversion

Guo-Yang Cao, Cheng Zhang, Shao-Long Wu, Dong Ma, Xiao-Feng Li

Citation: Chin. Phys. B. 2018, 27 (**12**): 124202 **doi:** 10.1088/1674-1056/27/12/124202
Journal homepage: http://cpb.iphy.ac.cn; http://iopscience.iop.org/cpb

What follows is a list of articles you may be interested in

Sub-external cavity effect and elimination method in laser self-mixing interference wave plate measurement system

Haisha Niu(牛海莎), Yanxiong Niu(牛燕雄), Jianjun Song(宋建军)
Chin. Phys. B . 2018, 27(2): 024201. **doi:** 10.1088/1674-1056/27/2/024201

Theoretical study of micro-optical structure fabrication based on sample rotation and two-laser-beam interference

Yizhen Chen(陈宜臻), Xiangxian Wang(王向贤), Ru Wang(王茹), Hua Yang(杨华), Yunping Qi(祁云平)
Chin. Phys. B . 2017, 26(5): 054203. **doi:** 10.1088/1674-1056/26/5/054203

Theoretical investigation of hierarchical sub-wavelength photonic structures fabricated using high-order waveguide-mode interference lithograph

Ru Wang(王茹), Xiangxian Wang(王向贤), Hua Yang(杨华), Yunping Qi(祁云平)

Chin. Phys. B . 2017, 26(2): 024202. **doi:** 10.1088/1674-1056/26/2/024202 **Second-order temporal interference of two independent light beams at an asymmetrical beam splitter**

Jianbin Liu(刘建彬), Jingjing Wang(王婧婧), Zhuo Xu(徐卓)
Chin. Phys. B . 2017, 26(1): 014201. **doi:** 10.1088/1674-1056/26/1/014201

Microtrap on a concave grating reflector for atom trapping

Hui Zhang(张 慧), Tao Li(李涛), Ya-Ling Yin(尹亚玲), Xing-Jia Li(李兴佳), Yong Xia(夏 勇), Jian-Ping Yin(印建平)
Chin. Phys. B . 2016, 25(8): 087802. **doi:** 10.1088/1674-1056/25/8/087802

SPECIAL TOPIC — Photodetector: Materials, physics, and applications

Physical manipulation of ultrathin-film optical interference for super absorption and two-dimensional heterojunction photoconversion*

Guo-Yang Cao(曹国洋)[1,2], Cheng Zhang(张程)[1,2], Shao-Long Wu(吴绍龙)[1,2], Dong Ma(马冬)[3,†], and Xiao-Feng Li(李孝峰)[1,2,‡]

[1] School of Optoelectronic Science and Engineering & Collaborative Innovation Center of Suzhou Nano Science and Technology Soochow University, Suzhou 215006, China

[2] Key Laboratory of Advanced Optical Manufacturing Technologies of Jiangsu Province, Key Laboratory of Modern Optical Technologies of the Education Ministry of China, Soochow University, Suzhou 215006, China

[3] School of Rail Transportation, Soochow University, Suzhou 215131, China

(Received 13 April 2018; revised manuscript received 12 September 2018; published online 10 November 2018)

Ultrathin optical interference in a system composed of absorbing material and metal reflector has attracted extensive attention due to its potential application in realizing highly efficient optical absorption by using extremely thin semiconductor material. In this paper, we study the physics behind the high absorption of ultrathin film from the viewpoint of destructive interference and admittance matching, particularly addressing the phase evolution by light propagation and interface reflection. The physical manipulations of the ultrathin interference effect by controlling the substrate material and semiconductor material/thickness are examined. We introduce typical two-dimensional materials — *i.e.*, MoS_2 and WSe_2 — as the absorbing layer with thickness below 10 nm, which exhibits $\sim 90\%$ absorption in a large range of incident angle ($0^\circ \sim 70^\circ$). According to the ultrathin interference mechanism, we propose the ultrathin (< 20 nm) MoS_2/WSe_2 heterojunction for photovoltaic application and carefully examine the detailed optoelectronic responses by coupled multiphysics simulation. By comparing the same cells on SiO_2 substrate, both the short-circuit current density (up to 20 mA/cm^2) and the photoelectric conversion efficiency (up to 9.5%) are found to be increased by $\sim 200\%$.

Keywords: photovoltaic, subwavelength structures, interference coating

PACS: 42.25.Hz, 78.66.–w, 88.40.H– **DOI:** 10.1088/1674-1056/27/12/124202

1. Introduction

Highly efficient optical absorption plays a fundamental role in a broad range of optoelectronic applications, including photoelectric conversion (*e.g.*, photodetection and photovoltaics),[1,2] photochemical cells,[3,4] light emission,[5,6] sensing,[7] *etc*. A photon-harvesting device without a good absorption can hardly obtain a high performance, no matter how the electrical conversion is optimized. Unfortunately, highly absorbing materials are always highly impedance-mismatched with air, leading to high reflection by the device surface.[8] Strengthened optical absorption can be achieved by employing the photonic designs. The most conventional strategy is to introduce single layer or multi-layer antireflection (AR) coatings composed of lossless dielectrics.[9] However, the AR layers need a quarter-wavelength in thickness, which hinders the miniaturizing of the optoelectronic devices (especially for infrared or far-infrared devices). Recently, with the rapid progress of nanofabrication technologies, the deep-subwavelength systems with broadband and high absorption (*e.g.*, those that are based on plasmonics or metamaterials) have been extensively studied and demonstrated.[10–14] Nevertheless, such systems largely rely on the precisely nanopatterning one or several layers, which require costly and complicated fabrication, thus hindering them from being used on a large-scale and lowing their cost in application.

Recently, a simple and ingenious solution based on antireflection principle was proposed to realize a broadband, wide-angle, and ultrahigh absorption in the ultrathin film with 10 nm–20 nm in thickness (far less than the quarter-wave thickness).[9,15–18] In the solution, 1) light-absorbing semiconductor replaces the conventional lossless dielectric material and 2) metal is used as back reflector. The special combination of highly absorbing semiconductor and metal reflector can greatly reduce the AR thickness because the reflection phase-shift introduced by the semiconductor/metal interface is significantly increased so that the required phase variation through the semiconductor becomes substantially small,

*Project supported by the National Natural Science Foundation of China (Grant Nos. 61675142 and 61875143), the Natural Science Foundation of Jiangsu Province, China (Grant No. BK20140359), the Natural Science Research Project of the Higher Educational Institutions of Jiangsu Province, China (Grant No. 17KJA480004), the Postgraduate Research & Practice Innovation Program of Jiangsu Province, China (Grant No. KYCX17_2027), and the Priority Academic Program Development of the Higher Educational Institutions of Jiangsu Province, China.

†Corresponding author. E-mail: madong@suda.edu.cn

‡Corresponding author. E-mail: xfli@suda.edu.cn

© 2018 Chinese Physical Society and IOP Publishing Ltd

allowing a much smaller thickness of the material. The unique thin-film planar scenario enables an extremely high absorption in the ultrathin semiconductor film. For example, Kats (Park) et al. reported that the 15 (12) nm Ge film on Au (Ag) substrate can absorb over 80% (98%) of light at a wavelength of $\lambda \sim 670$ (625) nm.[9,16] Such a planar system has also various applications, *e.g.*, in ultrathin color coatings,[9] broadband solar energy harvesting,[1,19] ultrathin devices based on van der Waals semiconductors,[15] *etc*. It has been indicated that the material and dimension of the metal and the semiconductor are critical for the ultrathin system to achieve high optical performance. Moreover, various deep-subwavelength film/metal systems under the same AR condition exhibit very distinguished optical absorbing performances. Therefore, more details of the fundamental optics within the ultrathin devices are required if we wish to better control the light coupling with the materials. In addition, the applications of this new system need to be further explored. For example, for the ultrathin solar cells, it is necessary to combine the superior optical performance with the realistic carrier transport/recombination process so that the complete optoelectronic performance of the device can be evaluated for a better device design.

In this paper, we first investigate the underlying optical mechanism responsible for the high absorption of the ultrathin semiconductor film on metal substrate, particularly addressing the phase evolution with the interface reflection and internal propagation, and also quantifying the phase condition for the destructive interference. The optical performances of the system under various semiconductor materials, semiconductor material thicknesses, and substrate materials are systematically studied. Moreover, an ideal substrate enables the system to possess the better absorption performance of the system than the systems under realistic metal or dielectric substrates. The scheme is further applied to a two-dimensional (2D) system with typical 2D materials, *i.e.*, MoS_2 and WSe_2, which exhibits nearly perfect absorption and good angular dependence with a material thickness below 10 nm. Finally, we design the ultrathin MoS_2/WSe_2 heterojunction for photovoltaic application with carefully examining the detailed optoelectronic responses, such as external-quantum efficiency (EQE) and current–voltage (J–V) curve. Compared with the same solar cell on conventional SiO_2 substrate, the short-circuit current density (J_{sc}) and photoelectric conversion efficiency (PCE) are both improved by $\sim 200\%$. The strong ultrathin-film interference provides the possibility of realizing miniaturized planar systems for high-performance, low-cost, and large-scale optoelectronic applications.

2. Device and method

A sketch of the ultrathin multilayer system is shown in Fig. 1(a), where N_1 $(= n_1 = 1)$, N_2 $(= n_2 + \mathrm{i}k_2)$ and N_3 $(= n_3 + \mathrm{i}k_3)$ are the complex refractive index of Air, α-Si, and Ag, respectively, and d is the thickness of the α-Si film. Initially, the α-Si film is considered as the absorbing AR layer on Ag (more material options to be determined later). Since the Ag layer is thick enough (much larger than the skin-depth of light in Ag), the substrate below Ag can be ignored; therefore, we refer to the Ag (or other metals) on the top of substrate as the Ag-substrate (or other metals) system. Considering that the light is perpendicularly incident onto the film from air, the optical response of the device is investigated by the Fresnel formula and transfer matrix method (TMM). The optical parameters of the materials under consideration are cited from the Palik table.[20]

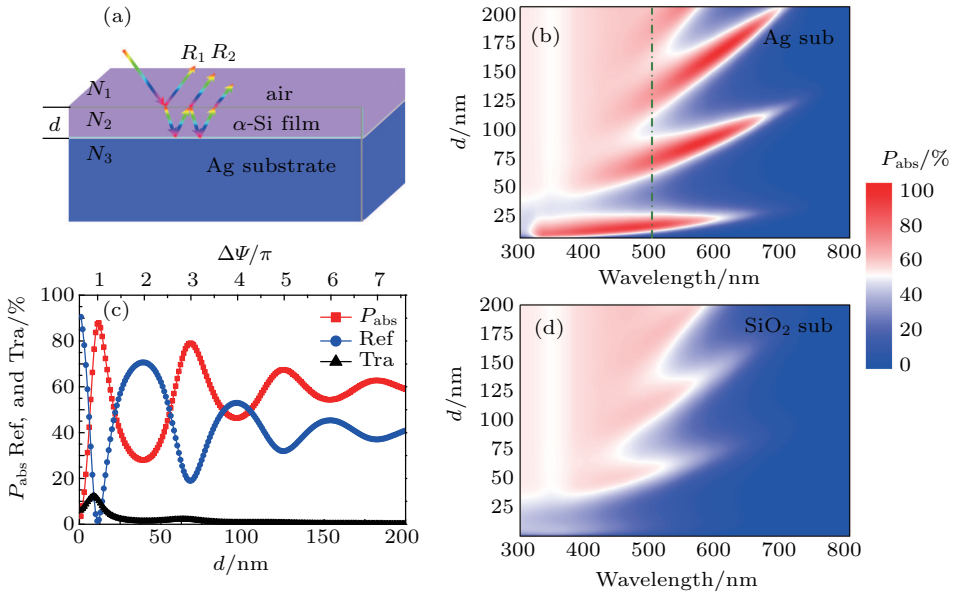


Fig. 1. (color online) (a) Sketch of device, where N_1, N_2, and N_3 are refraction indexes of air, α-Si, and Ag substrates, respectively. P_{abs} versus wavelength and α-Si thickness d on (b) Ag and (d) SiO_2 substrate under perpendicular incidence. (c) absorption, reflection, and transmission of the ultrathin film system versus d with $\lambda = 500$ nm. The top-x-axis shows corresponding $\Delta\Psi$.

We first briefly introduce the calculation process for studying the special optical interference in the ultrathin dielectric/metal system. The reflection coefficient and phase shift in the air/film (film/Ag) interface are denoted as r_{12} (r_{23}) and Ψ_{12} (Ψ_{23}), respectively, the phase accumulation in the thin film is represented by Ψ_d, and the phase difference between the direct surface reflection (R_1) and the reflected light by film/Ag after a round-trip propagation through the film (R_2) is denoted as $\Delta\Psi$ (without considering the high-order components). The phase change by interface reflection can be calculated by Fresnel formula. Note that the phase relation just considers the first-order propagation wave inside the ultrathin system. Given that the high-order components show dramatically reduced intensity, this treatment can approximate to the actual antireflection condition. Then we utilize TMM to calculate the optical response of the ultrathin system, including absorption ($P_{\rm abs}$), reflection (Ref), and transmission (Tra). The admittance of air, film, and substrate are η_1, η_2, and η_3, respectively. Note that the free space admittance (y_0) is taken to be the unit of admittance. The unpolarized sunlight absorption is modelled by the average of light absorptions under transverse-electric (TE, s-polarized) and transverse-magnetic (TM, p-polarized) incidence. The equivalent admittance of the whole system is η_z. The admittance difference between air and the system (*i.e.*, η_1 and η_z) is denoted as $\Delta\eta$.

3. Results and discussions

Figures 1(b) and 1(d) show the profiles of $P_{\rm abs}$ of the ultrathin α-Si film versus λ and d on Ag and SiO_2 substrates, respectively. It is obvious that: 1) both systems exhibit several absorption bands in the dispersion diagrams due to the excitation of various modes under destructive interference, and 2) the d value and the peak λ have a nearly linear relation, which can be explained by calculation formula of $\Psi_{\rm d}$. Moreover, the thinner absorbing layer leads the wider-band absorption to increase, which is beneficial to the design of many photoconversion devices such as the solar cells.[1,2] If we compare the results of the two systems based on Ag and SiO_2 substrates, the peaked absorption in the Ag system (Fig. 1(b)) is substantially higher than that of the SiO_2 system (Fig. 1(d)) due to the ultrathin optical interference effect as mentioned in the literature.[15–17]

Table 1. Values of d, $\Delta\Psi$, and $\Delta\eta$ at $M = 0$, 1, 2, and 3.

	$M=0$	1	2	3
d/nm	11	68	125	182
$\Delta\Psi$ (π)	1	3	5	7
$\Delta\eta$ (y_0)	0.21	1.5	2.6	3.1

At $\lambda = 500$ nm, the α-Si $P_{\rm abs}$, Ref, and Tra of the ultrathin α-Si/Ag system versus d are plotted in Fig. 1(c), where $\Delta\Psi$ is given to justify the interference situation. On the whole, $P_{\rm abs}$ and Ref oscillate with d in a contrary way and the absorption peaks (reflection dips) occur when $\Delta\Psi = (2M+1)\pi$ ($M = 0$, 1, 2, ...); *i.e.*, the destructive interference between the directly reflected light and the first order propagation light in the AR layer. Further study shows that the peaked $P_{\rm abs}$ decreases gradually with increasing d (*i.e.*, enlarging the order number m), which can be explained by the higher admittance mismatch $\Delta\eta$ between air and the system (see Table 1), weakening the AR effect despite the fact that the destructive phase condition is preserved. This suggests that the AR phase matching is not a sufficient condition for ultrahigh absorption because the admittance matching is also an important ingredient. In addition, the Ag substrate as a back reflector plays also a key role in enhancing absorption by efficiently restraining the transmission and elongating the light-path in the ultrathin film.

Figure 1(c) indicates that the $P_{\rm abs}$ peak of α-Si material at d of only 12 nm can reaches up to 90%. Such an outstanding light-trapping ability by an ultrathin semiconductor is due to the following reasons: 1) the phase change by the reflection of α-Si/Ag (air/α-Si) interface is 1.63π (1.02π); therefore, the phase accumulation in the α-Si layer is only 0.39π to satisfy the AR phase condition, allowing thickness to be very small—far less than the quarter wavelength; 2) there is a good admittance matching between the incident medium and the structure, and 3) Ag substrate reduces dramatically the transmission and enhances light-path in the ultrathin α-Si film.

Actually, for such an ultrathin system, the choice of back reflector is critical because it strongly affects the optical interference on the top surface. Moreover, as mentioned in Fig. 1, the ultrathin system can be used to achieve the broadband optical absorption; therefore, in the following, we introduce the AM1.5G solar illumination and evaluate the overall system performance by using the spectrally integrated photocurrent density $J_{\rm ph}$.[21] With an assumption of a perfect internal quantum process, which means that photo-generated carriers transform completely into output current, the photocurrent density $J_{\rm ph}$ can be calculated from $J_{\rm ph} = \int_{\lambda_1}^{\lambda_2} qF_{\rm S}(\lambda)P_{\rm abs}(\lambda)\,{\rm d}\lambda$, where λ_1 (λ_2) is the starting (cutoff) wavelength, q the electron charge, and $F_{\rm S}$ the spectral photon flux density of AM1.5G. Figure 2(a) shows the plots of $J_{\rm ph}$ versus d under ideal, Ag, Au, and SiO_2 substrate. Here, the ideal substrate is obtained by sweeping real and imaginary part of the substrate refractive index ($N_3 = n_3 + {\rm i}k_3$) at each thickness of α-Si layer. It is obvious that as a broadband absorber, the system with SiO_2 substrate shows fundamentally lower $J_{\rm ph}$, since the phase variation within the ultrathin α-Si layer is insufficient for AR interference. The Ag and Au substrates enable the AR effect to achieve much higher $J_{\rm ph}$ and comparably the Ag system can obtain the peak $J_{\rm ph} > 10$ mA/cm^2 at $d = 15$ nm; *i.e.*, a surprisingly high photocurrent by such an ultrathin semiconductor.

Nevertheless, the existing metals do not provide the best optical performance. It can be seen from Fig. 2(a) that the system with an optimized substrate can exhibit a $J_{ph} > 12$ mA/cm^2 with $d = 16$ nm.

To achieve a high J_{ph}, figure 2(b) reveals that n_3 has to be sufficiently small and k_3 has to be appropriately designed (see the inset of Fig. 2(b), where J_{ph} versus k_3 is shown with $n_3 = 0.01$). It suggests that the ideal $N_3 = 0.01+3.9i$ (denoted as Ideal sub 1 here). Correspondingly, figure 2(c) shows the map of the reflection phase change by the α-Si/substrate interface (*i.e.*, Ψ_{23}) at $\lambda = 500$ nm. Our calculation indicates that $\Psi_{23} = 1.54\pi$ and, therefore, $\Delta\Psi \sim 1.08\pi$ when using the Ideal sub 1, approximately satisfies the AR phase matching. There is a tiny difference from the calculated $\Delta\Psi$ (1.08π) in the ideal situation (π) since the design is for the full solar-spectrum absorption rather than the single AR wavelength. Figure 2(d) displays the P_{abs} spectrum of the α-Si film on Ideal sub 1 versus d, where the P_{abs} spectra at $d = 16$ nm with Ag and ideal substrates are compared in the inset. It is clear that the absorption ability of the ultrathin α-Si film on Ideal sub 1 is superior to that on the Ag substrate in a wide waveband.

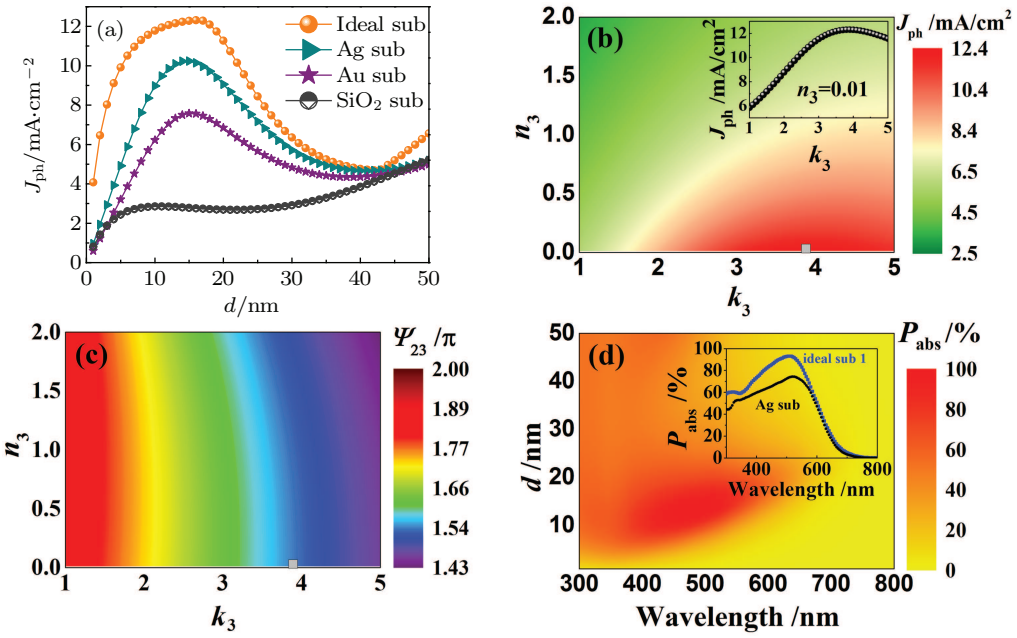


Fig. 2. (color online) (a) Plots of J_{ph} versus d on various substrates. (b) Plot of J_{ph} versus $N_3 (= n_3 + ik_3)$ with $d = 16$ nm, where inset shows plot of J_{ph} versus k_3 with $n_3 = 0.01$. (c) Reflection phase (Ψ_{23}) by the film/substrate interface. (d) Plots of P_{abs} versus d and wavelength with Ideal sub 1 ($N_{sub} = 0.01 + 3.9i$), where the inset shows plot of P_{abs} spectrum of system (with $d = 16$ nm) on Ideal sub 1 and Ag, respectively.

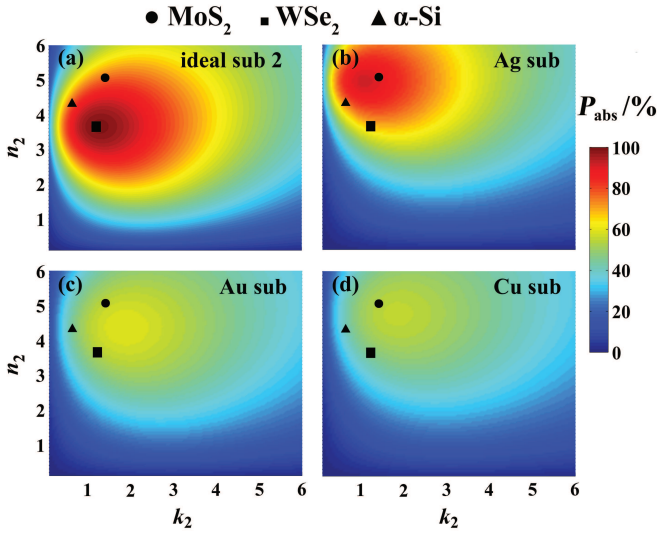


Fig. 3. (color online) P_{abs} versus N_2 $(= n_2 + ik_2)$ when $d = 9$ nm and $\lambda = 500$ nm respectively on (a) Ideal sub 2 ($N_{sub} = 0.01 + 1.36i$), (b) Ag, (c) Au, and (d) Cu substrate.

However, with the α-Si thickness decreasing into nano-size, the defect density of the ultrathin film becomes dramatically high[15] and this seriously limits the photoelectric conversion performance (despite the fact that the optical performance has been optimized significantly). Therefore, it is necessary to replace the conventional semiconductor material by the high-quality 2D materials; for instance, MoS_2, WSe_2, and other transition metal dichalcogenides layered materials (TMDLM). These 2D materials show many outstanding properties:[22–25] 1) no surface dangling bond, thus reducing the carrier loss caused by surface recombination, 2) strong light-absorbing ability [light is absorbed by the single layer MoS_2 (0.65 nm) is approximate to that of 50-nm-thick Si], and 3) reasonable and tunable bandgap by controlling the number of layers. In Fig. 3, we continually modulate the real and imaginary part of the refractive index of the AR material, *i.e.*, $N_2 = n_2 + ik_2$, and examine the absorption performances at a representative wavelength of 500 nm on various substrates (Ideal sub 2, Ag, Au, and Cu). Here, the thickness of the AR

layer is $d = 9$ nm and the Ideal sub 2 (with $N_3 = 0.01 + 1.36\mathrm{i}$) is designed by sweeping n_3 and k_3 under the given system configuration (similar to Fig. 2(b)). In these patterns, we can identify the materials of MoS_2, WSe_2, and α-Si according to their refractive index. It is found that the systems under Ideal sub 2 and Ag substrate show higher absorptions than those under the Au and Cu substrates. With Ideal sub 2 (Ag substrate), WSe_2 (MoS_2) system shows nearly unity absorption. The P_{abs} values under various AR and substrate materials are listed in Table 2.

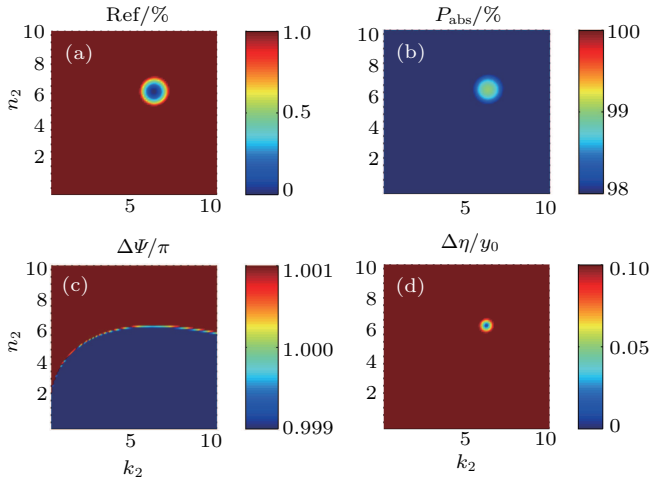


Fig. 4. (color online) Ref, P_{abs}, $\Delta\Psi$, and $\Delta\eta$ of 1 nm of film versus N_2 on ideal substrate ($N_3 = 0.01 + 0.01\mathrm{i}$) with 500 nm of perpendicular incidence.

Table 2. P_{abs} values under various film and substrate configurations, with film thickness $d = 9$ nm and perpendicular light wavelength 500 nm.

$P_{abs}/\%$		α-Si $N_2 = 4.37 + 0.65\mathrm{i}$	MoS_2 $N_2 = 5.1 + 1.42\mathrm{i}$	WSe_2 $N_2 = 3.66 + 1.23\mathrm{i}$
Sub	Ideal	77.02	74.9	99.1
	Ag	75.9	89.3	67.5
	Au	44.8	54.7	53.4
	Cu	40.8	53.5	46.1

By simultaneously modulating the film and substrate, it is found that even thinner film can obtain ultrahigh absorption. Figure 4(b) shows that 1-nm-thick ideal film on a designed substrate with $N_3 = 0.01 + 0.01\mathrm{i}$ can achieve $P_{abs} = 99\%$ under perpendicular incidence at the wavelength of 500 nm. Figure 4 also displays the corresponding Ref, $\Delta\Psi$, and $\Delta\eta$. It is shown that the reflection dip, absorption peak, phase relation under antireflection, and the admittance match happen at an identical N_2. Moreover, figure 4(c) indicates that there are many options for antireflection phase condition; however, the system does not show the corresponding high absorption or low reflection, indicating that the phase matching is just a necessary but not sufficient condition for antireflection effect.

Since the material is extremely thin, the angular performance is expected to be much higher than the angular performance of the conventional AR system.[19] Here, the TE and TM light incidence are taken into account and their average is used to mimic the non-polarized sunlight illumination. Figure 5 exhibits the angular response of P_{abs} of MoS_2 and WSe_2 ultrathin film with $d = 9$ nm and $\lambda = 500$ nm on Ideal sub 2 (Figs. 5(a) and 5(b)) and Ag substrate (Figs. 5(c) and 5(d)). From the figure, the P_{abs} value of MoS_2 and WSe_2 ultrathin film keep sufficiently high within a broad range of incident angle (0°–70°). This is because the phase responsible for the destructive interference comes mostly from the semiconductor/metal interface, rather than from the wave propagation in the AR layer; therefore, the AR effect can be roughly satisfied under different incident angles. The performance will be dramatically degraded only when the incident angle is sufficiently large ($\sim 80°$) due to the obvious phase mismatch.

Figure 5 also shows that the MoS_2 (WSe_2) ultrathin films absorb mainly the long (short) wavelength light; therefore, we can design the MoS_2/WSe_2 heterojunction ultrathin solar cell as an interesting application of the deep-subwavelength AR effect. When considering the solar cells, the detailed carrier dynamics during the generation, recombination, and collection in the device must be taken into account in order to evaluate the photoelectric performance accurately. The coupled optoelectronic simulation has been introduced to study various photoelectric devices in our previous research.[21,26–29] Here, we show the fundamental equations of the semiconductor model:

$$\nabla\cdot\left[-D_{\mathrm{n}}\nabla n + n\mu_{\mathrm{n}}\left(\nabla\Phi + \frac{\nabla\chi}{q} + \frac{k_{\mathrm{B}}T}{q}\nabla\ln N_{\mathrm{C}}\right)\right] = G(x,y,\lambda) - U, \tag{1}$$

$$\nabla\cdot\left[-D_{\mathrm{p}}\nabla p - p\mu_{\mathrm{p}}\left(\nabla\Phi + \frac{\nabla\chi}{q} + \frac{\nabla E_{\mathrm{g}}}{q} - \frac{k_{\mathrm{B}}T}{q}\nabla\ln N_{\mathrm{V}}\right)\right] = G(x,y,\lambda) - U, \tag{2}$$

$$\nabla^2\Phi = \frac{q}{\varepsilon_0\varepsilon_{\mathrm{r}}}(n - p + N_{\mathrm{A}} - N_{\mathrm{D}}), \tag{3}$$

where D_{n} (D_{p}) is the electron (hole) diffusion coefficient, μ_{n} (μ_{p}) the electron (hole) mobility, n (p) the electron (hole) concentration, N_{C} (N_{V}) the effective conduction (valence) band density of states, χ the electron affinity, Φ the electrostatic potential, T (300 K) the operating temperature, k_{B} the Boltmann's constant, E_{g} the band gap, ε_0 (ε_{r}) the vacuum permittivity (relative permittivity of the material), N_{D} (N_{A}) the donors (acceptors) concentration, and $G(x,y,\lambda)$ the carrier generation distribution, U the recombination. In the proposed heterojunction system comprised of 2D materials, the surface recombination can be ignored due to the absence of the surface dangling bond;[25] the bulk and interface recombinations include the contributions from Langevin and Shockley–Read–Hall (SRH) mechanisms.[26] Here we solve the Maxwell's equations, electron/hole transport equations, and Poisson's equation by the finite-element method (FEM) and finite-volume method (FVM) in COMSOL Multiphysics to obtain the photoelectric performance of the ultra-

thin MoS_2/WSe_2 heterojunction solar cell.[26] Since no high-dimensional nanopatterns are used in this system, the simulation can be performed by 2D models. The thickness of the multilayer MoS_2 and WSe_2 are 9.8 nm and 8.64 nm, respectively, and the key material parameters used in the simulation are cited from the literature.[24,26,30–41]

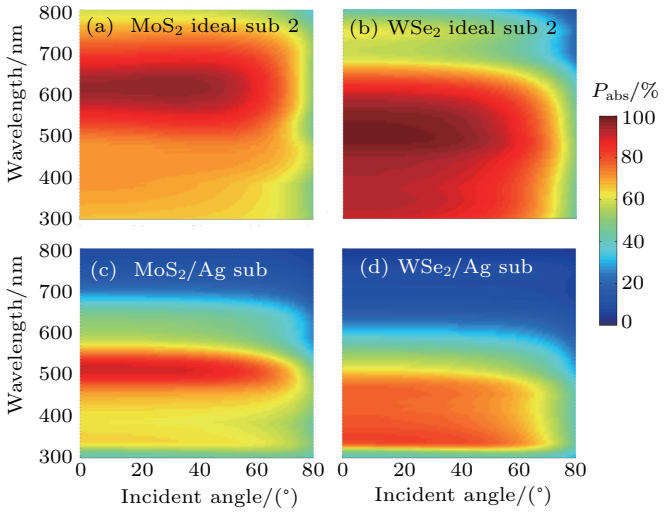


Fig. 5. (color online) Angular response of P_{abs} of MoS_2 and WSe_2 ultrathin film with $d = 9$ nm on (a) and (b) Ideal sub 2 and (c) and (d) Ag substrates.

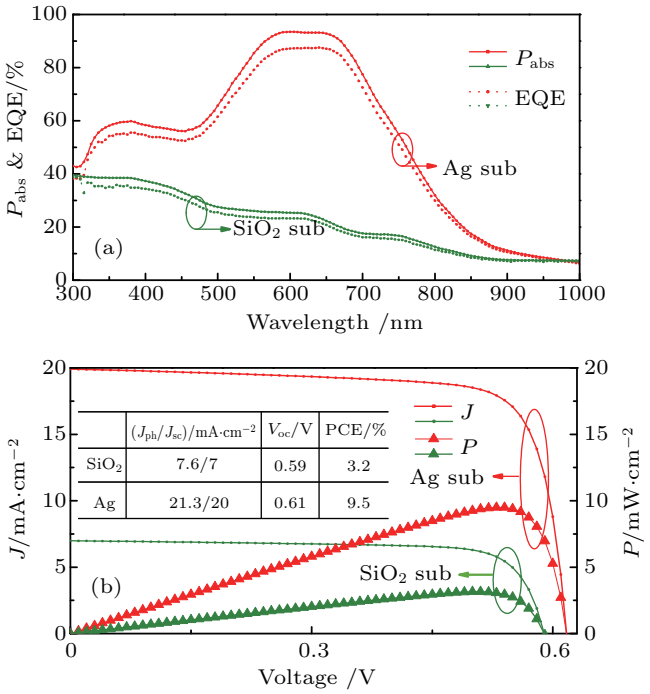


Fig. 6. (color online) (a) P_{abs} and EQE spectra of MoS_2/WSe_2 ultrathin heterojunction solar cell on Ag and SiO_2 substrates. (b) Corresponding J–V characteristics and output power density (P), where the typical performance parameters are inserted.

Figure 6(a) displays the P_{abs} and EQE spectra of the ultrathin MoS_2/WSe_2 heterojunction solar cells on Ag and SiO_2 substrates. It is clear that the improved optical response under the ultrathin interference effect is well transferred into the electrical domain, showing much higher EQE than the EQE of the conventional system with SiO_2 substrate. It should be mentioned that the ultrathin interference effect here is designed for the AR dual-layers, showing that the new optical scheme is applicable for the multilayer systems. Figure 6(b) shows the corresponding J–V curves under the two system configurations. Moreover, the optoelectronic performance parameters are inserted into the figure, in which the PCE $= (P_{max}/P_{in}) \times /\%$, where P_{max} $(= JV)$ is the maximal output power density and P_{in} (≈ 100 mW/cm^2) is the input power of AM1.5 solar illumination. These parameters include J_{ph}, J_{sc}, open-circuit voltage (V_{oc}), and PCE, which are 21.3 (7.6) mA/cm^2, 20 (7.0) mA/cm^2, 0.61 (0.59) V, and 9.5% (3.2%), respectively, for the proposed heterojunction solar cell on Ag (SiO_2) substrate. It is obvious that the photocurrent densities and the PCE are enhanced by almost 200% by utilizing the ultrathin interference effect. Interestingly, the heterojunction system with thickness less than 20 nm is predicted to show a PCE of 9.5%, which could be an opportunity for ultrathin high-performance photoconversion devices.

4. Conclusions

We have presented a comprehensive study on the ultrathin-film interference effect of the system, which is composed of strongly absorbing dielectric and back metal reflector, from the underlying physics, photonic manipulation, optical performance optimization, and also the photoconversion application. The transfer-matrix treatment, impedance matching condition, and the antireflection effect are used/discussed in detail. The various geometry and material options of the absorbing dielectric and substrate are considered through a comparable study of the system optical performance. It is found that the phase matching of antireflection is necessary but not a sufficient condition for ultrahigh absorption because the admittance matching is also an inevitable requirement. Particular attention is also paid to the incorporating of the 2D materials into this ultrathin-film system, which shows very good optical absorption in a large range of the incident angle. Finally, we construct an ultrathin MoS_2/WSe_2 heterojunction system for photovoltaic application. Under an AM1.5 solar illumination, the short-circuit current density, open-circuit voltage, and light-conversion efficiency of the proposed heterojunction on Ag (SiO_2) sub are 20 (7.0) mA/cm^2, 0.61 (0.59) V, and 9.5% (3.2%), respectively. Compared with the conventional system with dielectric substrate, the dielectric/metal setup shows the photocurrent density and PCE to be enhanced by $\sim 200\%$, thus promoting the practical application of TMDLM in photoelectric conversion.

References

[1] Piper J R and Fan S 2016 *ACS Photon.* **3** 571
[2] Pala R A, White J, Barnard E, Liu J and Brongersma M L 2009 *Adv. Mater.* **21** 3504

[3] Hasobe T, Fukuzumi S and Kamat P V 2006 *J. Phys. Chem. B* **110** 25477

[4] Lebedev N, Trammell S A, Dressick W, Kedziora G S, Griva I and Schnur J M 2011 *Photochem. Photobiol.* **87** 1024

[5] Yeh D M, Huang C F, Chen C Y, Lu Y C and Yang C C 2008 *Nanotechnol.* **19** 345201

[6] Sun G, Khurgin J B and Soref R A 2008 *J. Opt. Soc. Am. B* **25** 1748

[7] Kano H and Kawata S 1994 *Appl. Opt.* **33** 5166

[8] Rensberg J, Zhou Y, Richter S, Wan C, Zhang S, Schöppe P, Schmidt-Grund R, Ramanathan S, Capasso F, Kats M A and Ronning C 2017 *Phys. Rev. Appl.* **8** 014009

[9] Kats M A, Blanchard R, Genevet P and Capasso F 2013 *Nat. Mater.* **12** 20

[10] Yu N and Capasso F 2014 *Nat. Mater.* **13** 139

[11] Yao Y, Shankar R, Kats M A, Song Y, Kong J, Loncar M and Capasso F 2014 *Nano Lett.* **14** 6526

[12] Fang Z, Liu Z, Wang Y, Ajayan P M, Nordlander P and Halas N J 2012 *Nano Lett.* **12** 3808

[13] Echtermeyer T J, Britnell L, Jasnos P K, Lombardo A, Gorbachev R V, Grigorenko A N, Geim A K, Ferrari A C and Novoselov K S 2011 *Nat. Commun.* **2** 458

[14] Gilbertson A M, Francescato Y, Roschuk T, Shautsova V, Chen Y, Sidiropoulos T P, Hong M, Giannini V, Maier S A, Cohen L F and Oulton R F 2015 *Nano Lett.* **15** 3458

[15] Jariwala D, Davoyan A R, Tagliabue G, Sherrott M C, Wong J and Atwater H A 2016 *Nano Lett.* **16** 5482

[16] Park J, Kang J H, Vasudev A P, Schoen D T, Kim H, Hasman E and Brongersma M L 2014 *ACS Photon.* **1** 812

[17] Kats M A, Sharma D, Lin J, Genevet P, Blanchard R, Yang Z, Qazilbash M M, Basov D N, Ramanathan S and Capasso F 2012 *Appl. Phys. Lett.* **101** 221101

[18] Luo J, Li S, Hou B and Lai Y 2014 *Phys. Rev. B* **90** 165128

[19] Liu D, Yu H, Duan Y, Li Q and Xuan Y 2016 *Sci. Rep.* **6** 32515

[20] Palik E D 1985 *Handbook of Optical Constants of Solids* (San Deigo: Academic Press) USA, pp. 571–586

[21] Cao G, Li X, Zhan Y, Wu S, Shang A, Zhang C, Yang Z and Zhai X 2014 *Opt. Express* **22** A1761

[22] Wi S, Kim H, Chen M, Nam H, Guo L, Meyhofer E and Liang X 2014 *ACS Nano* **8** 5270

[23] Yin Z, Li H, Li H, Jiang L, Shi Y, Sun Y, Lu G, Zhang Q, Chen X and Zhang H 2011 *ACS Nano* **6** 74

[24] Radisavljevic B, Radenovic A, Brivio J, Giacometti I V and Kis A 2011 *Nat. Nanotechnol.* **6** 147

[25] Lee C H, Lee G H, Van Der Zande A M, Chen W, Li Y, Han M, Cui X, Arefe G, Nuckolls C, Heinz T, Guo J, Hone J and Kim P 2014 *Nat. Nanotechnol.* **9** 676

[26] Cao G, Shang A, Zhang C, Gong Y, Li S, Bao Q and Li X 2016 *Nano Energy* **30** 260

[27] Shang A, Zhai X, Zhang C, Zhan Y, Wu S and Li X 2015 *Prog. Photovolt.: Res. Appl.* **23** 1734

[28] Li X, Zhan Y and Wang C 2015 *Prog. Photovolt.: Res. Appl.* **23** 628

[29] Li X, Hylton N P, Giannini V, Lee K H, EkinsDaukes N J and Maier S A 2013 *Prog. Photovolt.: Res. Appl.* **21** 109

[30] Eichfeld S M, Eichfeld C M, Lin Y C, Hossain L and Robinson J A 2014 *APL Mater.* **2** 092508

[31] Yim C, O'Brien M, McEvoy N, Winters S, Mirza I, Lunney J G and Duesberg G S 2014 *Appl. Phys. Lett.* **104** 103114

[32] Liu H L, Shen C C, Su S H, Hsu C L, Li M Y and Li L J 2014 *Appl. Phys. Lett.* **105** 201905

[33] Bao W, Cai X, Kim D, Sridhara K and Fuhrer M S 2013 *Appl. Phys. Lett.* **102** 042104

[34] Das S, Chen H Y, Penumatcha A V and Appenzeller J 2012 *Nano Lett.* **13** 100

[35] Fang H, Chuang S, Chang T C, Takei K, Takahashi T and Javey A 2012 *Nano Lett.* **12** 3788

[36] Cui X, Lee G H, Kim Y D, Arefe G, Huang P Y, Lee C H, Chenet D A, Zhang X, Wang L, Ye F, Pizzocchero F, Jessen B S, Watanabe K, Taniguchi T, Muller D A, Low T, Kimv P and Hone J 2015 *Nat. Nanotechnol.* **10** 534

[37] Liu W, Kang J, Sarkar D, Khatami Y, Jena D and Banerjee K 2013 *Nano Lett.* **13** 1983

[38] Furchi M M, Pospischil A, Libisch F, Burgdörfer J, Mueller T 2014 *Nano Lett.* **14** 4785

[39] Britnell L, Ribeiro R M, Eckmann A, Jalil R, Belle B D, Mishchenko A, Kim Y J, Gorbachev R V, Georgiou T, Morozov S V, Grigorenko A N, Geim A K, Casiraghi C, Castro Neto A H and Novoselov K S 2013 *Science* **340** 1311

[40] Zhou S, Ye Y, Ding K, Jiang D, Dou X and Sun B 2018 *Chin. Phys. Lett.* **35** 066201

[41] Kadir N A A, Ismail E I, Latiff A A, Ahmad H, Arof H, & Harun S W 2017 *Chin. Phys. Lett.* **34** 014202